Distortional buckling of X-joints made of square hollow cross-section beams: theoretical energy-based model

Björk Timo, Ahola Antti, Tuominen Niko

DOI: 10.1002/stco.201800002

Distortional buckling of X-joints made of square hollow cross section beams: Theoretical energy-based model

Timo Björk*, Antti Ahola, Niko Tuominen

ABSTRACT

Current design codes do not consider distortional buckling failure modes, which can occur in the chord member of a tubular X-joint loaded axially by brace members. In this study, the critical load for distortional buckling is established based on the energy method and a beam on elastic foundation (BEF) approach. In the theoretical model, the capacity is created by elastic bending of the chord faces in their own planes and elastic bending of the cross section as a frame structure. The theoretical capacity of an X-joint is compared with numerical results obtained by finite element analyses (FEA). Some discrepancy is found between the theoretical model and numerical analysis, with the theoretical model slightly underestimating the load carrying capacity. Experimental tests show that an X-joint can be prone to distortional buckling failure mode. However, detailed scrutiny of distortional buckling failure in X-joints is only legitimate for joints made of high strength steel (HSS), because other failure mechanisms are more critical when conventional steels are used. Nevertheless, designers of X-joints with rectangular hollow section (RHS) members should be aware of this potential failure mode.

Keywords: tubular X-joints; rectangular hollow section; stability; ultimate capacity; distortional buckling

* Corresponding author. E-mail address: timo.bjork@lut.fi

1 INTRODUCTION

X-joints are typical structural details in tubular structures made of rectangular hollow sections (RHS) of the type illustrated in Fig. 1. Such joints are subjected to compression loading, and the capacity of the joint can be calculated according to Eurocode 3 (EC3) [1,2] or CIDECT design recommendations [3]. Figs 2a and 2b illustrate typical failure modes of joints with equal chord and brace width ($b_1 = b_0$). However, it is also theoretically possible that the web buckling does not occur symmetrically but asymmetrically, as illustrated in Fig. 2c, and the cross section of the chord member consequently distorts.

Fig. 1. Typical tubular structure with X-joints which can be subjected to axial compressive loading.

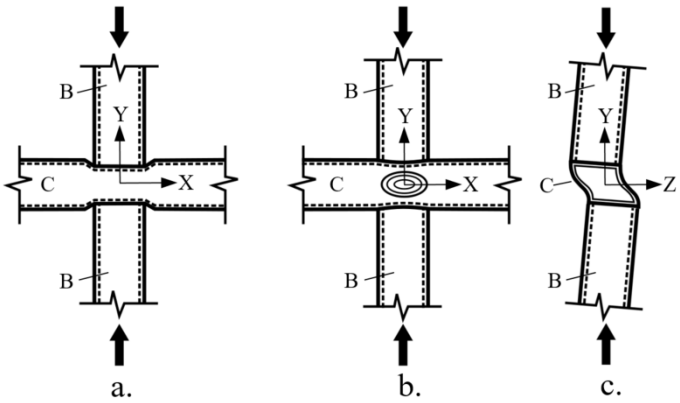

Fig. 2. Typical failure modes of compressed X-joints: a) chord flange failure, b) chord web symmetric buckling, and c) distortional buckling of chord member. B = brace member and C = chord member.

Distortion of a box cross section has been analyzed widely in the literature [4–11] but only to a limited extent from the stability point of view. Respectively, stability and ultimate capacity of RHS joints have been comprehensively analyzed [12–21] in terms of chord flange failure, chord web buckling and buckling of a brace member. In these papers, however, distortional buckling of a chord member was not investigated, or received little attention, since the studies mainly focused on RHS joints made of low strength steel, where the aforementioned failure mechanisms are more critical. Recently, Chen *et al.* [22] identified distortional buckling failure of a chord member in experimental tests carried out with axially compressed thin-walled RHS T- and X-joints, although this failure mechanism was not within the scope of the paper in general.

When tubular joints made of ultra-high strength steel (UHSS) are used, capacity to withstand chord flange yielding and chord web buckling failure modes increases and, as a consequence, distortional buckling of a chord member can become a critical mechanism. In this paper, a theoretical model for distortional buckling of tubular X-joints is formulated. The model is based on ideal elastic material behavior, and the results obtained by the theoretical model are compared with eigenvalues obtained by FEA. The criticality of distortional buckling mode against other failure mechanisms is evaluated and discussed.

2 THEORETICAL MODEL

The ideal elastic failure mechanism of a system that consists of two brace and chord members is illustrated in Fig. 3. All joint members are assumed to have rectangular hollow cross sections and the chord member has in this case a square hollow cross section (SHS) with nominal dimension $b_0 \times b_0 \times$ t and without corner rounding. Henceforth in this paper, the term “SHS” is used to describe the chord member, although the fabrication process of

the hollow section can be either forming or welding. The X-joint is prepared with pure single-bevel butt welds and the weld has thus no geometrical influence on the general joint behavior. However, welds have a significant local boundary effect on the chord flanges, which prevent the free deformation of the flanges in the line of welds. However, this local irregularity is ignored in this simplified analyses. The welding is assumed to have not such a metallurgical effect on the material properties, which could affect the ideal-elastic capacity of the joint. The center line of the wall thickness is used as the calculation dimension, i.e. $b = b_0 - t$. The brace members are pin-ended at the loading ends but free to move in the direction of the loading. The chord member is only fixed in the joint area. The loss of stability does not occur by the free distortion mode of a chord member but the brace members control the cross section deformation of the chord member in the joint area.

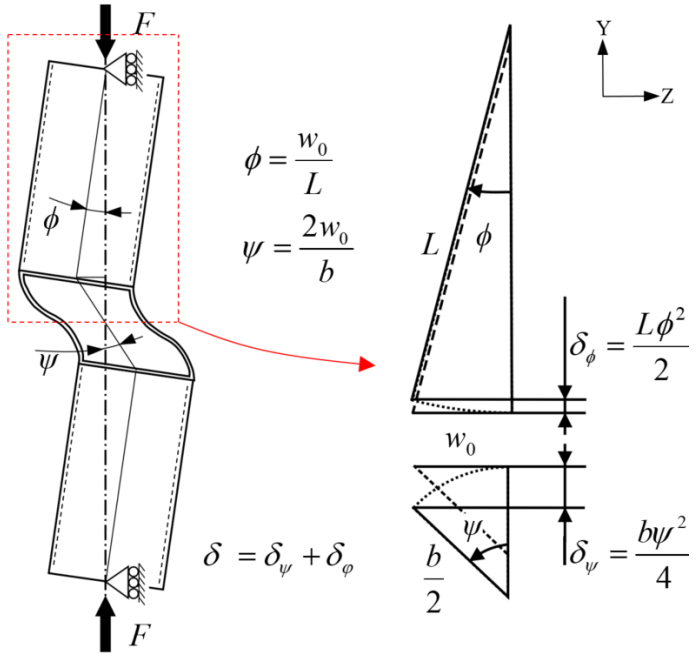

Fig. 3. Distortional failure mechanisms and dimensions in the compressed X-joint, upper half of the mechanism is illustrated on the right side figure.

If the axial rigidity of the brace members is assumed to be large compared to the other terms, the axial deformation at the end of the brace members, δ, consists of the rigid body movement of the brace member and the deformation of the chord. Consequently, the potential energy of the system is [23]:

$$V = -2F\delta = -2F\left[L(1-\cos\psi) + \frac{b}{2}(1-\cos\phi) \right]. \quad (1)$$

Because the bifurcation occurs by small lateral displacement, also the angles (ϕ, ψ) are small, and Eq. (1) can be re-formulated:

$$V \approx -2F\left[L\frac{\psi^2}{2} + \frac{b}{2}\frac{\phi^2}{2} \right] = -F\left[\frac{1}{L} + \frac{2}{b} \right] w_0^2. \quad (2)$$

The axial force F is the only external loading of the system and w_0 is the asymmetric lateral displacement due to the chord deformation. The other geometrical symbols are given in Fig. 3.

The deformed joint is loaded, in addition to the compression force F, by a horizontal couple force F_h, as illustrated in Fig. 4. This couple force can be divided into pure torsional and distortional loadings. Consequently, the chord corner deformation consists of torsional ($w_t = v_t$) and distortional ($w_d = v_d$) components. Because in this case the chord member is not supported outside the joint area, the torsional forces (Fig. 4b) are in equilibrium with the bending moment and shear force of the brace members. However, the effects of these brace loadings on the deformation of the joint and on the strain energy of the system can be ignored. Moreover, as the Bredt's torsion moment occurs only at the joint area of the chord member and outside the joint, only the distortional components exist (Fig. 4c).

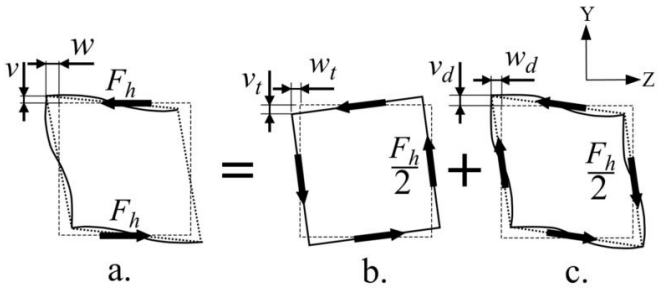

Fig. 4. a) Forces and deformation of chord cross section consist of b) Bredt's torsion and c) distortion.

The matching of deformations in the brace and chord corners introduces the following requirement:

$$v = \frac{b}{2L} w . \tag{3}$$

Furthermore, the following Eqs. are valid in the joint area:

$$v = v_d - v_t = \frac{b}{2L} w \quad \rightarrow \quad v_t = w_t = v_d - \frac{b}{2L} w = w_d - \frac{b}{2L} w \tag{4}$$

$$w = w_t + w_d = w_d - \frac{b}{2L} w + w_d \tag{5}$$

$$w_d = v_d = \frac{2L + b}{4L} w \tag{6}$$

$$w_t = v_t = \frac{2L - b}{4L} w . \tag{7}$$

The linear elastic strain energy due to the distortion of the chord member is:

$$U_d = \frac{1}{2}\left[4\int_0^{\infty} \frac{Etb^3}{12}\left(\frac{d^2 w_d}{dx^2}\right)^2 dx + 4\int_0^{\infty} \frac{Etb^3}{12}\left(\frac{d^2 v_d}{dx^2}\right)^2 dx \right] + 16\int_0^{\infty}\left[\frac{12(1-\nu^2)}{Et^3} \int_0^{\frac{b}{2}} \frac{m_s^2}{2} ds \right] dx , \tag{8}$$

where E is Young's modulus, ν is Poisson's ratio and d^2/dx^2 denotes the second derivative of the horizontal and vertical displacements (w_d, v_d) of the faces (and corners) of the distorted

cross section, respectively. The two first terms represent the bending of flanges and webs about their major axis when the corners of the cross sections are assumed to be idealized hinges as illustrated in Fig. 5. The strain energy involved in twisting of the cross section faces is neglected, because the elastic torsional constant ($bt^3/3$) is fractional compared to the elastic bending resistance of the plate ($b^3t/12$).

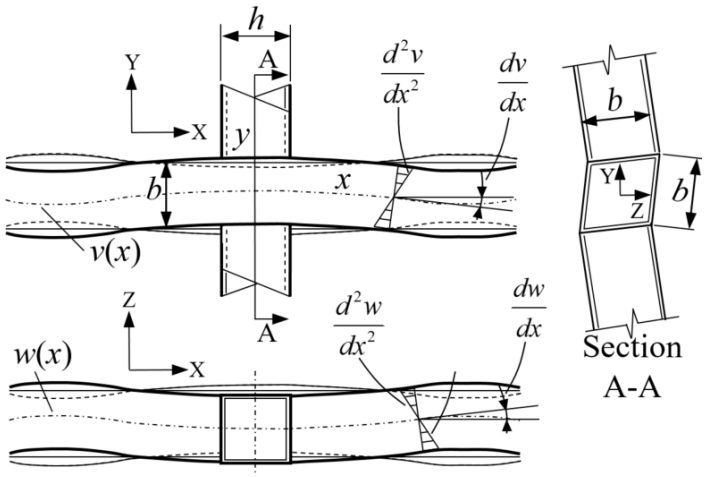

Fig. 5. Distortional warping of the cross section with the hinged corners.

Because the longitudinal displacement *u* for the flange and web is equal in the corners of the cross section and the distortional displacement functions are equal for asymmetric SHS deformations, the second derivatives for horizontal and vertical deformations are also equal, and the two first terms can be merged, giving:

$$U_d = \frac{1}{2}\left[8\int_0^{\infty}\frac{Etb^3}{12}\left(\frac{d^2w_d}{dx^2}\right)^2 dx\right] + 16\int_0^{\infty}\left[\frac{12(1-\nu^2)}{Et^3}\int_0^{\frac{b}{2}}\frac{m_s^2}{2}ds\right]dx. \qquad (9)$$

The second term in Eq. (9) represents the transverse bending moment m_s of the flanges and webs about their minor axis as seen in Fig. 6. This term considers the real corner stiffness

and this deformation is required for having continuous displacements along the cross section perimeter.

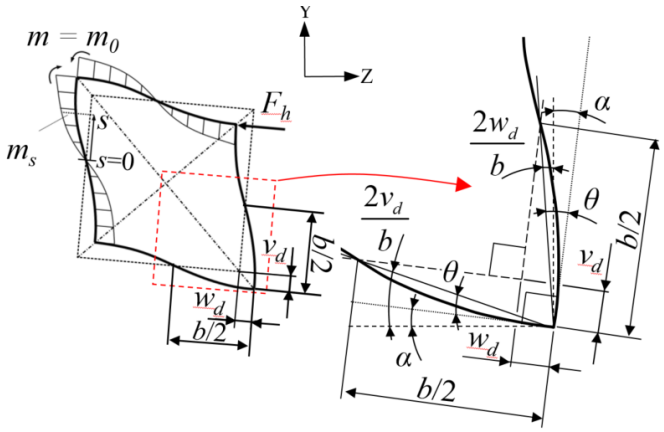

Fig. 6. Distortion of cross section as a frame structure and moments in flange and web of the cross section.

The corners of the box section remain rectangular in shape and consequently:

$$\alpha = \frac{2w_d}{b} - \theta = \theta - \frac{2v_d}{b} \rightarrow \theta = \frac{w_d + v_d}{b} = \frac{2w_d}{b} = \left(\frac{1}{b} + \frac{1}{2L}\right) w \,. \tag{10}$$

In the corner, the transverse moment $m_s = m_0$ is:

$$m_0 = \frac{6Et^3}{12\left(1-\nu^2\right)b}\theta = \frac{Et^3}{\left(1-\nu^2\right)b^2} w_d \,. \tag{11}$$

The transverse moment distribution m_s along the local cross section coordinate s is:

$$m_s = \frac{2s}{b} m_0 = \frac{2Et^3 w_d}{\left(1-\nu^2\right)b^3} s \,. \tag{12}$$

The strain energy contained in the frame moment m_s can now be calculated as follows:

$$\int_0^{\frac{b}{2}} \frac{m_s^2}{2} ds = \int_0^{\frac{b}{2}} \frac{E^2 t^6 w_d^2}{\left(1-\nu^2\right)^2 b^6} s^2 ds = \frac{E^2 t^6}{24\left(1-\nu^2\right)^2 b^3} w_d^2 \tag{13}$$

In addition to the distortion, strain energy also exists due to the twisting of the chord member, as shown in Fig. 4. Thus:

$$U_t = \frac{1}{2}\left[4\int_0^{\infty} \frac{GI_t}{b^2}\left(\frac{dw_t}{dx}\right)^2 dx + 4\int_0^{\infty} \frac{EI_\omega}{b^2}\left(\frac{d^2 w_t}{dx^2}\right)^2 dx \right], \tag{14}$$

where G is shear modulus, and I_t and I_ω are torsional and warping constants of the chord member, respectively. In this case, the chord is free to rotate along its longitudinal axis and, consequently, the first and second derivative of twisting angle are zero, and thus U_t = 0. Additionally, the primary torsional warping constant of a SHS is zero, if the effect of potential corner radius is ignored as found out by Rubin [24]. The secondary torsional warping constant is numerically insignificant (= $t^3b^3/36$). However, in the general case, the total strain energy stored in the torsion of cross section, consisting of free torsion and primary- and secondary torsional warping and distortional warping, must be considered. In this case the total energy Π contained in distortional buckling of the X-joint is:

$$\Pi = V + U_d + U_t = -F\left[\frac{1}{L} + \frac{2}{b}\right] w_0^2 + \frac{Etb^3}{3}\int_0^{\infty}\left(\frac{d^2 w_d}{dx^2}\right)^2 dx + \int_0^{\infty} \frac{8Et^3}{\left(1-\nu^2\right)b^3} w_d^2 dx. \tag{15}$$

Total energy of the system is in equilibrium when Π = 0. The distortional buckling of the X-joint can be analyzed based on the beam on elastic foundation (BEF) theory presented by Timoshenko [25]. Consequently, the distortional displacement for an infinite beam loaded by concentrated load $F_h/2$ is:

$$w_d = \frac{F_h \lambda}{4k} e^{-\lambda x}\left(\sin \lambda x + \cos \lambda x\right) \tag{16}$$

and the second derivative thus is:

$$\frac{d^2 w_d}{dx^2} = \frac{F_h \lambda^3}{2k} e^{-\lambda x}\left(\cos \lambda x - \sin \lambda x\right). \tag{17}$$

Fig. 7 shows the relative distribution of the distortional displacement and the second derivative as a function of λx (without constant factors).

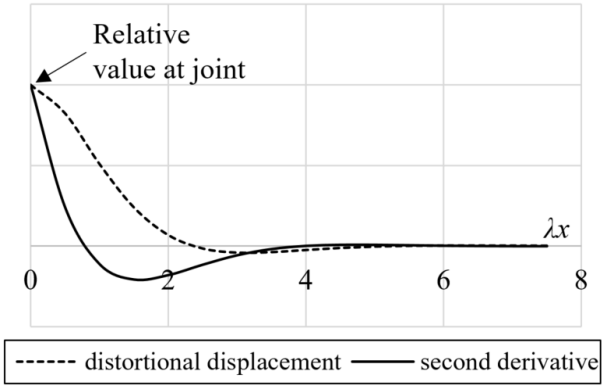

Fig. 7. Distribution of distortional deformation and its second derivative.

The elastic foundation stiffness factor k can be defined from Eq. (11):

$$m_0 = \frac{F_h}{4}\frac{b}{2} = \frac{Et^3}{\left(1-\nu^2\right)b^2} w_d \tag{18}$$

$$\frac{F_h}{2} = \frac{4Et^3}{\left(1-\nu^2\right)b^3} w_d = k w_d \tag{19}$$

$$k = \frac{4Et^3}{\left(1-\nu^2\right)b^3} \quad . \tag{20}$$

The characteristic parameter λ is [26]:

$$\lambda = \sqrt[4]{\frac{k}{4E\dfrac{b^3 t}{12}}} = \sqrt[4]{\frac{12t^2}{\left(1-\nu^2\right)b^6}} \quad . \tag{21}$$

The total horizontal displacement at the joint ($x = 0$) can be obtained from Eqs. (5) and (16):

$$w_0 = \frac{4L}{2L+b} w_{d,0} = \frac{L}{2L+b}\frac{F_h \lambda}{k}. \tag{22}$$

By substituting Eqs (16), (17) and (20) into (15) and considering the trigonometrical equivalences, the critical load can be defined:

$$F_{cr} = \left(2+\frac{b}{L}\right) bEt \left[\frac{b^3\lambda^4}{12} \int_0^\infty e^{-2\lambda x}\left(1-\sin 2\lambda x\right)dx + \frac{t^2}{2\left(1-\nu^2\right)b^3} \int_0^\infty e^{-2\lambda x}\left(1+\sin 2\lambda x\right)dx \right]. \tag{23}$$

The integrations can be carried out analytically obtaining the result [27]:

$$F_{cr}=\left(2+\frac{b}{L}\right)bEt\left[\begin{array}{l}\dfrac{b^3\lambda^3}{48}\Big|_0^{\infty}\left[e^{-2\lambda x}\left(\sin 2\lambda x+\cos 2\lambda x-2\right)\right]\\ -\dfrac{t^2}{8\left(1-\nu^2\right)\lambda b^3}\Big|_0^{\infty}\left[e^{-2\lambda x}\left(\sin 2\lambda x+\cos 2\lambda x+2\right)\right]\end{array}\right]. \tag{24}$$

Substituting the integration limits, the critical load of the joint is given:

$$F_{cr}=\left(2+\frac{b}{L}\right)bEt\left[\frac{b^3\lambda^3}{48}+\frac{3t^2}{8\left(1-\nu^2\right)\lambda b^3}\right] \quad . \tag{25}$$

However, the theoretical treatment neglects the local effect of the joint. The local behavior of the joint is very complex but its effect on the load capacity can be estimated by a simplified model of the joint. For the purposes of simplification, the distortion deformation w_d is assumed to be constant over the joint length h and also its second derivative is assumed also to be constant (which is slightly in conflict with the previous statement), as illustrated in Fig. 8.

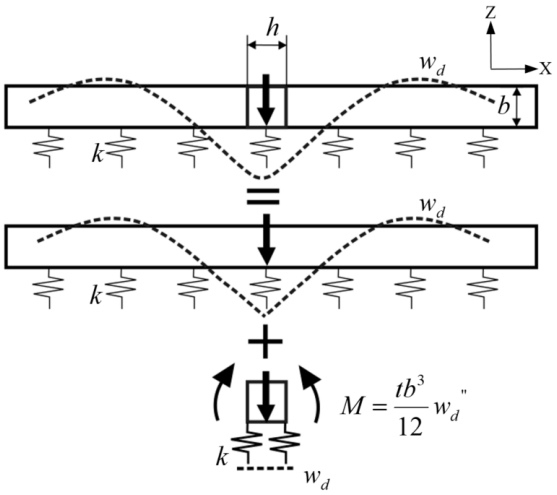

Fig. 8. A simplified model to consider the local effect of joint.

The additional strain energy at the joint area can be considered using Eqs. (9), (13), (16) and (17). The linear elastic distortional buckling load of the X-joint is:

$$F_{cr} = \left(2 + \frac{b}{L}\right) bEt \left[\frac{b^3 \lambda^3}{48} (1 + 2\lambda h) + \frac{t^2}{8(1-\nu^2)\lambda b^3} (3 + 2\lambda h) \right] \quad (26)$$

3 NUMERICAL SIMULATIONS

3.1 FE-model

The X-joint described in Section 2 was analyzed numerically using the Abaqus 2016 program. The geometries and cross section classes of analyzed profiles are shown in Table 1. The cross section classes of RHS depend on the steel grade and slenderness ratio of the flat part in the chord web.

Table 1. Analyzed cross sections of X-joint with equal brace and chord members.

Section	SHS X-joint b_0/t	Ratio c/t_0	Classification of the steel section according to EN 1993-1-1 Steel grade and f_y / $R_{p0.2}$ [MPa]					
			235	275	355	460	550	≥690
100 × 3	33.3	29.3	1	1	2	2	4	4
150 × 3	50	46	4	4	4	4	4	4
150 × 4	37.5	33.5	2	2	3	4	4	4
150 × 5	30	26	1	1	1	2	3	4
200 × 6	33.3	29.3	1	1	2	3	4	4
Limit	≤ 35	ε:	1	0.924	0.814	0.715	0.654	≤0.584
EN 1993-1-8 [1], Table 7.8		EN 1993-1-1 [28], Table 5.2: Class 1: $c/t \leq 33\varepsilon$; Class 2: $c/t \leq 38\varepsilon$: Class 3: $c/t \leq 42\varepsilon$ with $\varepsilon = (235 \text{ MPa} / f_y)^{1/2}$ For SHS, EN 10219-2 [29]: $c = b_0 - 2r_0$ or $c = b_0 - 2(t_0+r_i)$ with $r_o = 2t_0$ and $r_i = t_0$ for $t_0 \leq 6$ m; with $r_o = 2.5t_0$ and $r_i = 1.5t_0$ for 6 mm < $t_0 \leq 10$ mm or with $r_o = 3t_0$ and $r_i = 2t_0$ for $t_0 > 10$ mm						

The boundary conditions and applied loads were modeled to be identical with the idealized theoretical model. The element model used is presented in Fig. 9. The element type was linear quadrilateral plate elements (S4R). The element size was set as 10 mm x 10 mm in each model. A seed load of 1 N was applied in the center of the brace section and the edges of the brace sections were coupled with the center of the sections using a kinematic coupling constraint. The models were defined as a mid-surface model. Young's modulus and Poisson's ratio of 210 GPa and 0.3 were used, respectively.

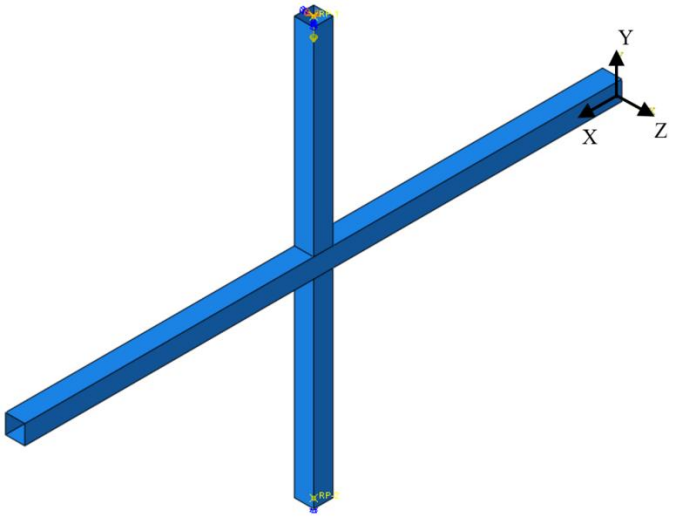

Fig. 9. Geometry of a FE-model.

No weld was modeled, and the joint was completely fixed around the brace member perimeter, which makes the joint area stiffer than the theoretical model. Both eigenvalue and nonlinear analyses were carried out.

3.2 Eigenvalue analyses

All cases were calculated using brace lengths L =250 to 2000 mm with 250 mm as step length for the four different SHS dimensions. The cross sections and obtained eigenvalue results are presented in Fig. 10.

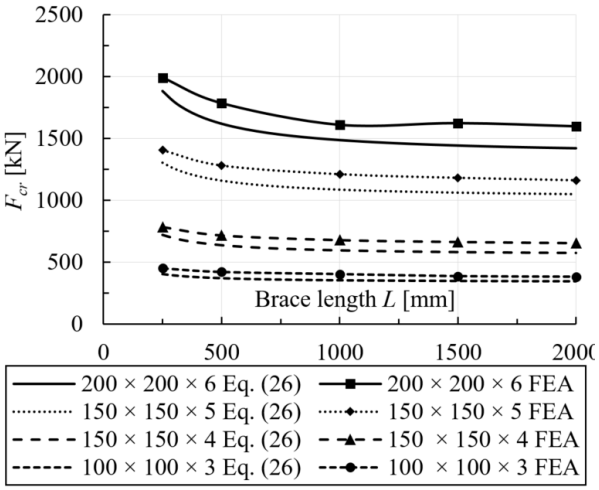

Fig. 10. Results from the FEA and analytical results.

Fig. 11 illustrates joint behavior in the distortional buckling mode. The rigid body rotation of the chord member induced by Bredt's torsional moment is clearly seen at the free edges of the chord member. Furthermore, the oscillation effect of distortion in the longitudinal direction of the chord member can also be seen in Fig. 11.

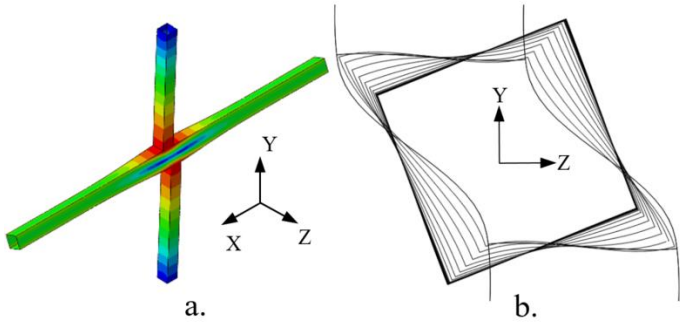

Fig. 11. Set of cross section deformations of chord member through the joint area.

3.3 Nonlinear analyses

Nonlinear analyses for an X-joint made of ultra-high strength steel were carried out to find out the criticality of this failure mechanism compared to other potential modes, see Fig. 2.

An X-joint with dimensions of 150 × 150 × 5 [mm] was chosen for these analyses since a corresponding experimental test result was available (see Section 4). The element type and size were similar to those used in the eigenvalue analyses, but geometrically and materially nonlinear analyses (GMNA) were nevertheless carried out. The same values were used for Young's modulus and Poisson's ratio as in the eigenvalue analyses. Bi-linear material properties were applied based on information given by the tube manufacturer, see Table 2.

The X-joint was analyzed with three different angular misalignments of the brace member, γ = 0, 1° and 2°. The chord length was 1000 mm and the brace length 850 mm, resulting in a total length of 1850 mm, see Fig. 12. The obtained ultimate loads F_u and the failure modes of the analyses are presented in Table 2. The force-displacement curves of the geometrically and materially nonlinear analyses (GMNAs) are shown in Fig. 13 with the experimental curve (Section 4).

Table 2. Material properties and results of nonlinear analysis of X-joints with equal brace and chord members with SHS 150 × 150 × 5. Strain value corresponds with f_u.

Case ID	Yield strength f_y [MPa]	Ultimate Strength f_u [MPa]	Strain [-]	Misalignment of the brace γ [degree]	Ultimate load F_u [kN]	Failure mode
1				0	1302	Chord web buckling
2	1080	1299	0.089	1	1005	Distortional buckling
3				2	901	Distortional buckling

Based on these preliminary investigations, it becomes clear that distortional buckling is a more critical failure mode for high-strength steels than mild steels, because compressed X-joints made of low or mild steels are prone to global yielding rather than distortional buckling.

4 EXPERIMENTAL TESTS

Experimental tests specific to distortional buckling of the chord member were not carried out within this study. However, a test with an X-joint made of 150 × 150 × 5 mm S960MC RHS showed the susceptibility of such joints to distortional buckling, as can be seen in Fig. 12.

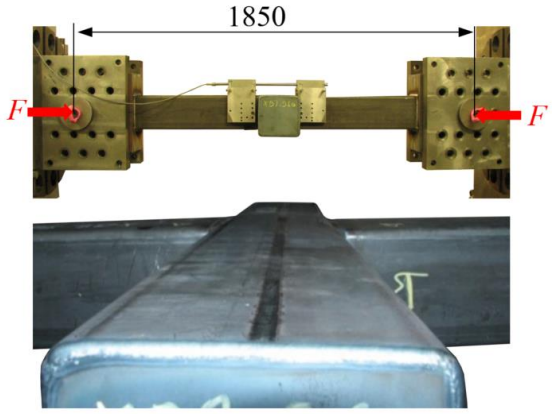

Fig. 12. Distortion of X-joint after unloading of the applied compression load.

The final failure mode found in the test was elastic web buckling, but there was clearly interaction with the distortional mode. The load-displacement curves of the test and GMNAs are presented in Fig. 13.

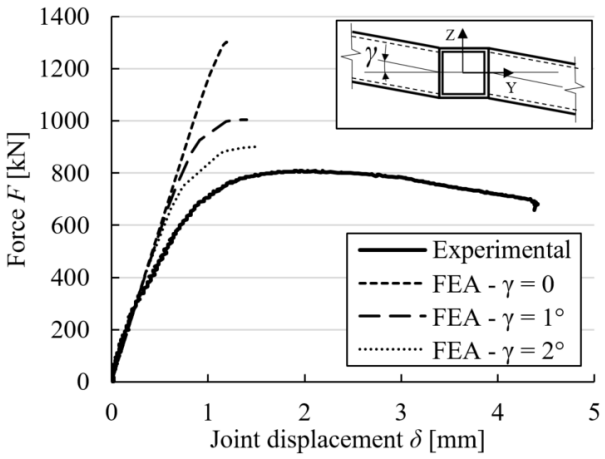

Fig. 13. Force-displacement curves for X-joints made of 150 × 150 × 5 S960 CFSHS in comparison with the curves obtained by the FEA.

Although the brace members were nominally pin-ended, in practice there was remarkable friction, providing extra support at the ends of the brace members. It was not the initial aim of the test to study distortional buckling, rather other failure modes were expected. In light of the outcome of the test, in future tests, the brace members will be longer and real pin-ended fixing will be used. According to the analytical model, Eq. (26), the critical load for this joint is 1087 kN while the ultimate capacity was 800 kN in the test.

5 DISCUSSION

5.1 Geometrical parameters

The analytical model demonstrates the effects of essential geometrical parameters on the load carrying capacity of the joint. The wall thickness t has, of course, a clear and important role in the load carrying capacity. The dimension b has two conflicting effects. Extending the outer dimensions of the cross section increases the bending resistance of the chord faces in their own plane but weakens the out-of-plane bending stiffness; b^3 appears in both terms, see Eq. (25). The brace length L has relatively small influence on the capacity.

The selected boundary condition at the ends of the chord member can be called into question. However, the use of free ends is reasonable since it is the natural boundary condition for the case of adjacent similar joints, as illustrated in Fig. 1. Likewise, pin end fixing of the brace member is a natural boundary condition if the brace length L is half of the distance between adjacent chord members.

It is quite interesting to note from Fig. 7 that the bending moments (= second derivative of the displacement) of the chord faces the decrease quicker than the distortional displacement. From Eq. (16) the first zero-level passing should occur for the tested X-joint at distance x:

$$\sin \lambda x + \cos \lambda x = 0 \quad \rightarrow \quad x = \frac{\arctan(-1)}{\lambda} = \frac{3\pi}{4\lambda} = 965 \text{ mm}.$$

The chord was not long enough to reach this situation freely. The moment reaches its first zero-level at a distance of 322 mm. Hence, the distortion affects the chord quite significantly.

5.2 Comparison with FEA

The analytical model underestimates the load carrying capacity compared to numerical results obtained by FEA. One reason for the difference can be the complicated joint area, which is stiffer in the FEA than the theoretical model. The joint can be modified in the FEA and laboratory tests to correspond better to the theoretical model by creating a gap between the brace and chord members at the chord flange area. This would demonstrate the role of local boundary conditions to the distortional capacity of the joint. The bending moment of the brace members could be included in the theoretical model, but this addition would lead to overestimation of the role of the brace length and complicate the analyses. Longer brace member are more flexible, allowing Bredt's rotation to occur more easily in the joint.

Neglect of brace members may be one reason why the FEA results deviate from the analytical capacities. In order to improve the accuracy of this analysis, more sophisticated type of elements should be used as proposed for e.g. by van der Vegte [30], particularly in the case of nonlinear analyses. The effect of element type on the ideal elastic buckling capacity, tested in one of the analyzed geometries, was approximately 2%.

5.3 Validity

The design codes generally assume elastoplastic failure or buckling to determinate governing failure modes for the design. For a design of SHS-X-joints, the range of validity is limited to side slenderness ratios $b/t \leq 35$ and the elastic-plastic cross sections of class 1 to 2 (for chord generally and for braces under compression only) for steel grades up to S460 (with further restrictions and currently under discussion up to S700). The restrictions usually prevent other, non-plastic failure modes, which are not covered in the design codes. However, if cross sections are beyond the range on validity, and especially with high- and ultra-high strength steels, distortional buckling should be considered. However, assessment of design load for distortional buckling needs more numerical and experimental investigations over a wide range of geometrical and material parameters. Li [31] investigated different types of tubular joints in a master's thesis and assessed validations for web- and distortional buckling as shown in Fig. 14.

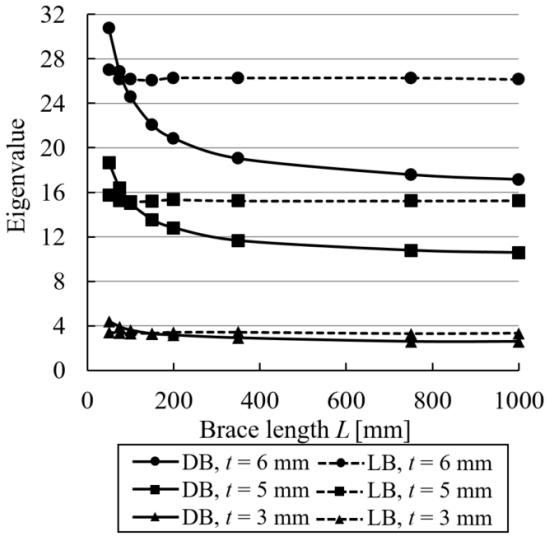

Fig. 14. Local buckling and distortion buckling eigenvalues of SHS 150 × *t*. DB = distortional buckling and LB = local web buckling of chord member [29].

Furthermore, the role of geometrical imperfection is essential. The effects of initial distortion of the chord member and asymmetric axial and angular misalignments between brace and chord members are an important consideration in validation of this failure mode. Preliminary effects of angular misalignment on the load carrying capacity of an X-joint can be seen in Fig. 13. It should , however, be noted that with normal joint geometries, distortional buckling need only be considered when high strength steels are used because similar joints made of low strength or mild steel will fail by elastoplastic failure and buckling mechanisms. Tubular joints made of high- or ultra-high strength steel have hitherto not been widely used, which is probably the reason why such failures have not occurred or been reported in practice. However, Chen *et al.* [22] conducted tests for X-joints made of 50 × 50 × 1.1 mm SUS304 stainless steel RHS (f_y = 375 MPa and f_u = 575 MPa) with equal brace and chord widths, i.e. $b_0 = b_1$, and found distortional buckling of chord member to be a potential failure mode for tubular joints. It appears that the tubular structures made of high strength steels can be prone to a distortional buckling mode that can be ignored in the case of low strength steels.

5.4 Future work

Future work will focus on the validation of this failure mode by carrying out experimental tests and nonlinear FEA. In both methods, the real material model and effect of imperfections, such as presented in design codes [28,29], on the ultimate capacity will be considered. In addition, the competitive distortional failure modes, considering different joint configurations, will be under theoretical investigation.

6 CONCLUSIONS

In this study, a theoretical model for distortional buckling was presented. Based on the results, the following conclusions can be drawn:

- Distortional buckling can theoretically be a critical mode and it should thus be considered during design.
- The theoretical model provides a good overview of the geometrical effects on the ideal elastic capacity of X-joint distortional buckling.
- The FEA results match theoretical models quite well; however, the current theoretical model seems to underestimate the capacity slightly.
- A method to deduce design capacity from ideal elastic capacity is still lacking.
- Potential distortional buckling deserves attention when using high strength steel.
- Extension of the presented theory to a wider range of applications and further experimental tests are required.

ACKNOWLEDGEMENTS

This work was supported by SSAB, DIMECC Ltd. and the Finnish Funding Agency for Innovation (TEKES) in the BSA (Breakthrough Steels and Applications) program. Additionally, the authors express their gratitude to the IT Center for Science (CSC) for software licensing and to Dr.-Ing. I. Pertermann for valuable technical advice.

BIBLIOGRAPHY

[1] EN 1993-1-8. Eurocode 3 - Design of steel structures - Part 1-8: Design of joints, 2005.

[2] EN 1993-1-12. Eurocode 3 - Design of steel structures - Part 1-12: Additional rules for the extension of EN 1993 up to steel grades S700, 2007.

[3] Packer, J. A.; Wardenier, J.; Zhao, X. L.; van der Vegte, G. J.; Kurobane Y.: *Design Guide for Rectangular Hollow Section (RHS) Joints Under Predominatly Static Loading*. LSS Verlag; 2009. doi:10.1016/S0034-3617(10)70040-0.

[4] Vlasov, V. Z.: *Thin-walled Elastic Beams*. Jerusalem: Israel Program for Scientific Translations; 1963.

[5] Kollbrunner, C. F.; Hajdin, N.: *Dünnwändige Stäbe, Band 2: Stäbe mit deformierbaren Querschnitten Nichtelastisches Verhalten dünnwandiger Stäbe*. Berlin: Springer-Verlag Berlin Heidelberg; 1975. doi:10.1007/978-3-662-06782-6.

[6] Kristek, V.: *Theory of Box Girders*. Prague: John Wiley & Sons Ltd; 1979.

[7] Kähönen, A.; Niemi, E.: Distortion of a double symmetric box section subjected to eccentric loading - using the beam on elastic founding approach. Research report. Lappeenranta University of Technology; 1986.

[8] Schardt, R.: *Verallgemeinerte Technische Biegetheore*. Berlin: Springer-Verlag Berlin Heidelberg; 1989. doi:10.1007/978-3-642-52330-4.

[9] Saoula, A.; Meftah, S. A.; Mohri, F.; Daya, E. M.: Lateral buckling of box beam elements under combined axial and bending loads. *Journal of Constructional Steel Research* **116** (2016), pp. 141–55. doi:10.1016/j.jcsr.2015.09.009.

[10] Fan, Z.; Helwig, T.: Distortional loads and brace forces in steel box girders. *Journal of Structural Engineering* **128** (2002), No. 6, pp. 710–718. doi:10.1061/(ASCE)0733-9445(2002)128:6(710).

[11] Ahlfors, M.: Distortion and internal warping torsion of a double symmetric hollow section. Master's thesis, Lappeenranta University of Technology. 2015.

[12] Matsui, C.; Morino, S.; Kawano, A.: Lateral-torsional buckling of trusses with rectangular tube sections. Welding of Tubular Structures, Proceedings of 2nd International Conference, Boston: Pergamon Press, 1984, pp. 101-108. doi:10.1016/B978-0-08-031156-2.50015-4.

[13] Zhao, X. L.: Deformation limit and ultimate strength of welded T-joints in cold-formed RHS sections. *Journal of Constructional Steel Research* **53** (2000), pp. 149–165. doi:10.1016/S0143-974X(99)00063-2.

[14] Rasmussen, K.; Young, B.: Tests of X- and K-Joints in SHS stainless steel tubes. *Journal of Structural Engineering* **127** (2001), pp. 1173–1182.

[15] Basaglia, C.; Camotim, D.: Buckling analysis of cold-formed RHS frames using generalized beam theory. In: Young, B. (ed.): Proceedings of the 13th International Symposium on Tubular Structures, Hong Kong: CRC Press, 2010, pp. 187-195. doi:10.1201/b10564-27.

[16] Feng, R.; Young, B.: Experimental investigation of cold-formed stainless steel tubular T-joints. *Thin-Walled Structures* **46** (2008), pp. 1129–1142. doi:10.1016/j.tws.2008.01.008.

[17] Feng, R., Young, B.: Design of cold-formed stainless steel tubular T- and X-joints. *Journal of Constructional Steel Research* **67** (2011), 421–436. doi:10.1016/j.jcsr.2010.09.011.

[18] Mohan, M.; Wilkinson, T.: FEA of T & X joints in grade C450 steel. In: Gardner, L. (ed.): Proceedings of the 14th International Symposium on Tubular Structures, Leiden: CRC Press, 2012, pp. 185–194.

[19] Becque, J.; Wilkinson, T.: Experimental investigation of the static capacity of grade C450 RHS T and X truss joints. In: Gardner, L. (ed.): Proceedings of the 14th International Symposium on Tubular Structures: CRC Press; 2012, pp. 177–184.

[20] Becque, J.; Wilkinson, T.: A new design equation for side wall buckling of RHS truss X-joints. In: Batista, E.; Vellasco, P.; Lima, L. (eds): Proceedings of the 15th International Symposium on Tubular Structures, Leiden: CRC Press, 2015, pp. 419–426.

[21] Yu, Y.: The static strength of uniplanar and multiplanar connections in rectangular hollow sections. Master's thesis, Delft University of Technology. 1997.

[22] Chen, Y.; Feng, R.; Fu, L.: Investigation of grouted stainless steel SHS tubular X- and T-joints subjected to axial compression. *Engineering Structures* **150** (2017), pp. 318–333. doi:10.1016/j.engstruct.2017.07.052.

[23] Allen, H. G.; Bulson, P. S.: *Background to Buckling*. London: McGraw-Hill Inc.; 1980.

[24] Rubin, H.: Torsions-Querschnittswerte für rechteckige Hohlprofile nach EN 10210-2 : 2006 und EN 10219-2 : 2006. Stahlbau 2007;76:21–33. doi:10.1002/stab.200710004.

[25] Timoshenko, S.: *Strength of Materials. Part II. Advanced Theory and Problems*. 3rd ed. New York: D. Van Nostrand Company; 1958.

[26] Wrigth, R. N., Abdel-Saman, S. R.; Robinson, A. R.: BEF analogy for analysis of box girders. *Journal of Structural Division* **94** (1968), pp. 1719–1744.

[27] Beyer, W. H., Selby, S.: *Standard Mathematical Tables*. 24th ed. Ingram; 1976.

[28] EN 10219-2. Cold formed welded structural hollow sections of non-alloy and fine grain steels - Part 2: Tolerances, dimensions and sectional properties, 2018.

[29] EN 1993-1-1. Eurocode 3: Design of steel structures - Part 1-1: General rules and rules for buildings, 2005.

[30] van der Vegte, A., Wardenier, J., Puthli, R.: FE analysis for welded hollow-section joints and bolted joints. *Structures and Buildings* **163** (2010), pp. 427–37.

[31] Li, L.: Distortion buckling analysis of rectangular hollow sections X-joints using finite element method. Master's thesis. Lappeenranta University of Technology, 2013.

D. Sc. (Tech.) Timo Björk, Professor

M. Sc. (Tech.) Antti Ahola, Junior Researcher

M. Sc. (Tech.) Niko Tuominen, Junior Researcher

Lappeenranta University of Technology

Laboratory of Steel Structures

P.O. Box 20

FI-53851 Lappeenranta

Finland